

NUMERICAL SIMULATION OF THE SIMULTANEOUS PRECIPITATION OF δ AND γ' PHASES IN THE NI-BASE SUPERALLOY ATI ALLVAC@718 PLUS™

Rene Radis^{1,2}, Gerald A. Zickler³, Martin Stockinger⁴, Christof Sommitsch^{2,5}, Ernst Kozeschnik¹

¹Christian Doppler Laboratory “Early Stages of Precipitation”, Institute of Materials Science and Technology, Vienna University of Technology, Favoritenstraße 9-11, Vienna, 1040, Austria

²Institute for Materials Science and Welding, Graz University of Technology,
Kopernikusgasse 24, Graz, 8010, Austria

³Christian Doppler Laboratory “Early Stages of Precipitation”, Montanuniversität Leoben,
Franz-Josef-Straße 18, Leoben, 8700, Austria

⁴Böhler Schmiedetechnik GmbH & Co KG, Mariazeller-Straße 25, Kapfenberg, 8605, Austria

⁵Christian Doppler Laboratory “Materials Modelling and Simulation”, Institute for Materials
Science and Welding, Graz University of Technology,
Kopernikusgasse 24, Graz, 8010, Austria

Keywords: nickel-base superalloys, ATI Allvac@718 Plus™, precipitation kinetics, delta,
gamma prime, numerical simulations

Abstract

The present work deals with the numerical simulation of the precipitation kinetics of δ ($\text{Ni}_3(\text{Nb}, \text{Al})$) and γ' ($\text{Ni}_3(\text{Al}, \text{Ti}, \text{Nb})$) phases in the commercial nickel-base superalloy ATI Allvac@718Plus™. Important precipitate parameters such as volume fraction, mean radius and number density are numerically calculated as a function of the heat treatment parameters time and temperature and compared to experimentally determined data. To match the experimentally observed kinetics, the predicted interfacial energy of the precipitates, as calculated for a sharp, planar phase boundary, is adjusted to take into account the interfacial curvature and entropic effects of a diffuse interface. Using these modified interfacial energies, the calculated results show excellent agreement with the experimental measurements. Finally, a calculated time-temperature-precipitation (TTP) diagram for concurrent δ and γ' precipitation is presented, which clearly demonstrates strong kinetic interactions during simultaneous precipitation of these phases. Thus, the present study emphasizes the importance of carefully controlling the heat treatment parameters time and temperature during the production process of ATI Allvac@718Plus™, in order to achieve the desired microstructure and hence mechanical properties.

Introduction

The term superalloy is generally used for a large number of different alloys. A major motivation for the development of nickel-based superalloys is their applicability for gas turbine components in aircrafts and power plants. The degree of the turbine efficiency increases with increasing operation temperatures. Usually, Ni-base superalloys combine high strength and good corrosion resistance, which are essential for the application in modern gas turbine aero-engines, e.g. for high-speed rotating components, such as high-pressure turbine disks [1].

A novel representative of these nickel-base alloys is the superalloy ATI Allvac®718Plus™ (718Plus™ is a trademark and Allvac® is a registered trademark of ATI Properties, Inc., Monroe, NC, USA), which is a further development of the classical alloy 718 [2]. Compared to alloy 718, the new alloy contains cobalt, tungsten, a higher amount of aluminum and less iron and titanium, see Table I. According to the chemical composition of ATI Allvac®718Plus™, the most essential precipitates in this alloy are the D0_a-ordered δ (Ni₃(Nb,Al)) and the L1₂-ordered γ' (Ni₃(Al,Ti,Nb)) phases. The precipitation of a suitable quantity and size of coarse δ precipitates is used for controlling grain growth [3,4], whereas the precipitation of a large amount of fine-dispersed coherent γ' precipitates provides strengthening by precipitation hardening [5,6]. Therefore, knowledge of the precipitation kinetics of both phases is of high technological interest in order to control the evolution of microstructure during processing and to achieve the desired material properties.

In the present work, the precipitation behavior of the δ and γ' phases is studied numerically and compared to corresponding experiments. A series of isothermal precipitation kinetics simulations at different temperatures is carried out employing the thermo-kinetic software MatCalc. Furthermore, the competition of the alloying elements Nb and Al during precipitation is discussed. Finally, a complete time-temperature-precipitation (TTP) diagram for δ and γ' phases is determined, which provides important information on heat treatments for alloy ATI Allvac®718Plus™ in order to achieve the desired microstructure and mechanical properties.

Table I: Chemical composition (wt%) of alloy 718 and ATI Allvac®718Plus™ [3].

alloy	Ni	Ti	Al	Nb	Cr	Co	Fe	Mo	W	C
alloy 718	base	1.0	0.5	5.4	18.1	-	18.0	2.9	-	0.03
ATI Allvac®718Plus™	base	0.7	1.5	5.4	18.0	9.0	10.0	2.7	1.0	0.03

Computer Simulations

For the simulation of the precipitation kinetics of the phases δ and γ' in ATI Allvac®718Plus™, the thermo-kinetic software MatCalc (version 5.30 rel 1.036) [7,8,9] is used. The thermodynamic description and the diffusion data are taken from refs. [10,11]. In this approach, the nucleation kinetics of precipitates is calculated from classical nucleation theory (CNT) [12,13] extended for multi-component systems [7,13,14]. Accordingly, the transient nucleation rate J is given as

$$J = N_0 Z \beta^* \cdot \exp\left(\frac{-G^*}{k \cdot T}\right) \cdot \exp\left(\frac{-\tau}{t}\right). \quad (1)$$

J describes the rate at which nuclei are created per unit volume and time. N_0 represents the total number of potential nucleation sites. The Zeldovich factor Z considers that the nucleus is destabilized by thermal excitation as compared to the inactivated state. The atomic attachment rate β^* takes into account the long-range diffusive transport of atoms, which is needed for nucleus formation if the chemical composition of the matrix is different from the chemical composition of the precipitate. T is the temperature, k the Boltzmann constant and t the time. The incubation time τ is given as [12]

$$\tau = \frac{1}{2\beta^* Z^2}, \quad (2)$$

and the critical energy for nucleus formation G^* is

$$G^* = \frac{16\pi}{3} \frac{\gamma^3}{\Delta G_{\text{vol}}^2}, \quad (3)$$

with the effective interfacial energy γ and the volume free energy change ΔG_{vol} . It is important to note that G^* is the most essential quantity in the nucleation equation (1) when compared to the other components. G^* contains the cube of the interfacial energy over the square of the driving force ΔG_{vol} . Since G^* appears in the exponent of the nucleation rate equation (1), small changes in γ and/or ΔG_{vol} can lead to significant variations in J , which is demonstrated in a treatment of the evolution of multimodal size distributions in the nickel-base superalloy UDIMET 720 Li [15].

Once a precipitate is nucleated, its further growth is evaluated based on the evolution equations for the radius and composition of the precipitate derived by Svoboda et al. [7] in a mean-field approach utilizing the thermodynamic extremal principle. Accordingly, the growth rate $\dot{\rho}_k$ and the rate of change of chemical composition \dot{c}_{ki} of the precipitate with index k are obtained from solution of the linear system of equations

$$A_{ij} y_j = B_i, \quad (4)$$

where the variable y_j represents the rates $\dot{\rho}_k$ and \dot{c}_{ki} , as well as the Lagrange multipliers from the stoichiometry constraints (see reference [7]).

The system of equations (4) is solved for each precipitate k separately. The full expressions for the coefficients A_{ij} and B_i , as used in the present work, are given in reference [9]. The numerical time integration of $\dot{\rho}_k$ and \dot{c}_{ki} is performed in the software package MatCalc, based on the classical numerical Kampmann – Wagner approach [16], and it is described in detail in reference [8]. The interfacial energy is calculated from a generalized n -next nearest-neighbor broken-bond approach [17], assuming a planar, sharp interface, shown as dotted lines in Figure 1.

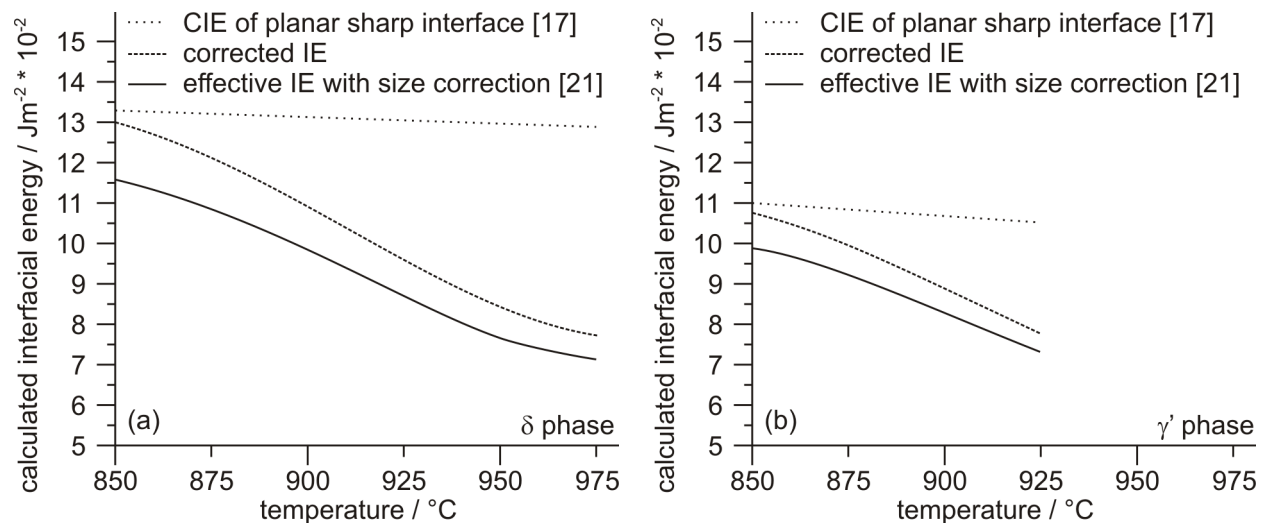


Figure 1: Calculated interfacial energy (CIE) for a planar sharp interface [17] (dotted lines) and corrections accounting for entropic contributions from finite interface thickness (dashed lines) and interfacial curvature [21] (solid lines), for the phases δ (a) and γ' (b).

However, particularly, close to the solution temperature, the effect of entropic contributions from finite interface thickness can become prominent. This behavior of the interfacial energy has been observed in previous works by Pudar et al. [18] in the case of Nb(C,N) as well as by Radis and Kozeschnik [19] for VN and treated theoretically in ref. [20]. Taking into account entropic contributions (dashed lines) and the size correction for the spherical shape of the nucleus [21] an effective interfacial energy during the nucleation stage may be calculated, see solid lines in Figure 1. The nucleation of both phases is assumed to occur at dislocations, preferentially, with a dislocation density of 10^{11} m^{-2} [22].

With this approach, a series of calculations at different annealing temperatures is carried out and compared with the experimental data.

Results and Discussion

The precipitation kinetics of δ and γ' phases in ATI Allvac®718Plus™ is simulated at various temperatures. Figure 2 shows the calculated equilibrium phase fractions at temperatures between 800 °C and 1100 °C. In equilibrium, both phases are stable at temperatures below 975 °C, where the following precipitation kinetic simulations are performed.

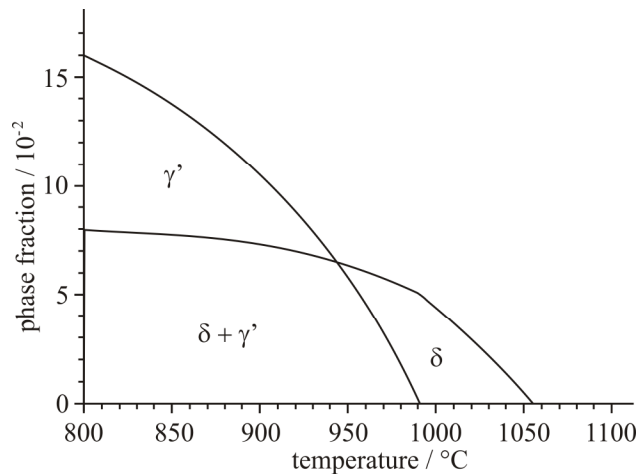


Figure 2: Calculated equilibrium phase fractions of δ and γ' precipitates at temperatures between 800 °C and 1100 °C [23].

Figure 3 depicts the calculated δ and γ' phase fractions versus time with experimental results of δ phase precipitation at temperatures between 850 °C and 975 °C [23]. The solid lines represent the phase fraction of the δ phase, whereas the dashed lines indicate the phase fractions of the γ' phase. The filled circles indicate the experimental data of the δ phase, obtained according to the procedure described in ref. [3]. The calculations at the two highest temperatures (Figure 3(a,b)) show that only the δ phase is predicted to appear within a given time span. With decreasing temperature, precipitation of γ' is observed and the kinetics becomes faster with lower temperatures. At a temperature of 875 °C (Figure 3(e)), the precipitation of both phases occurs simultaneously. After decreasing the temperature to 850 °C (Figure 3(f)), partial redissolution follows rapid precipitation of γ' , supporting growth of the δ phase.

In addition to the precipitation of the δ phase, the evolution of the γ' phase is also simulated and compared to experimental information obtained by SANS (small-angle neutron scattering) investigations [24]. Figure 4 shows numerical simulations and experimental data for radius, number density and volume fraction of the γ' precipitates as a function of time for aging

temperatures of 875 °C (Figure 4(a-c)) and 825 °C (Figure 4(d-f)). The solid lines show the precipitate parameters of the γ' phase and the dashed lines indicate the phase fraction of the δ phase. In the simulations, the identical heat treatments are simulated as experimentally performed in reference [24]. The simulations in Figure 4 include the solution heat treatment at 1010 °C and a heating ramp of 100 °C min⁻¹ to the respective aging temperatures. This is in contrast to the simulations and experimental data in Figure 3 which use differing parameters resulting in differences in predicted and experimental precipitation behavior between Figures 3 and 4.

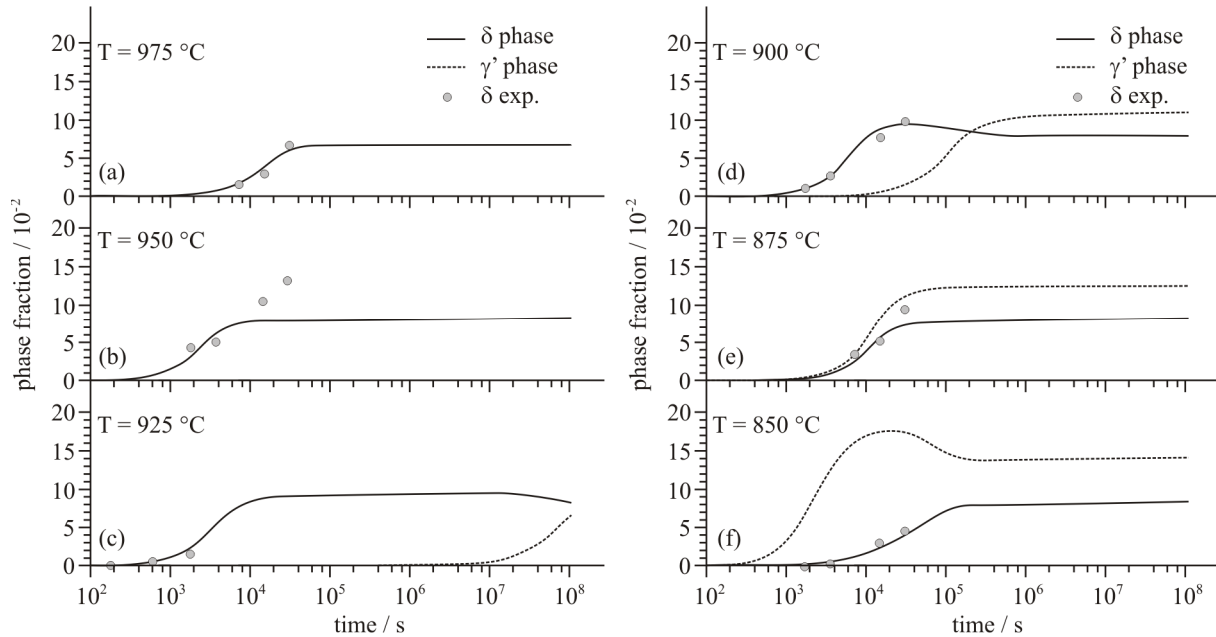


Figure 3: Calculated δ and γ' phase fractions versus log time and comparison with experimental results of δ phase at temperatures between 850 °C and 975 °C [23].

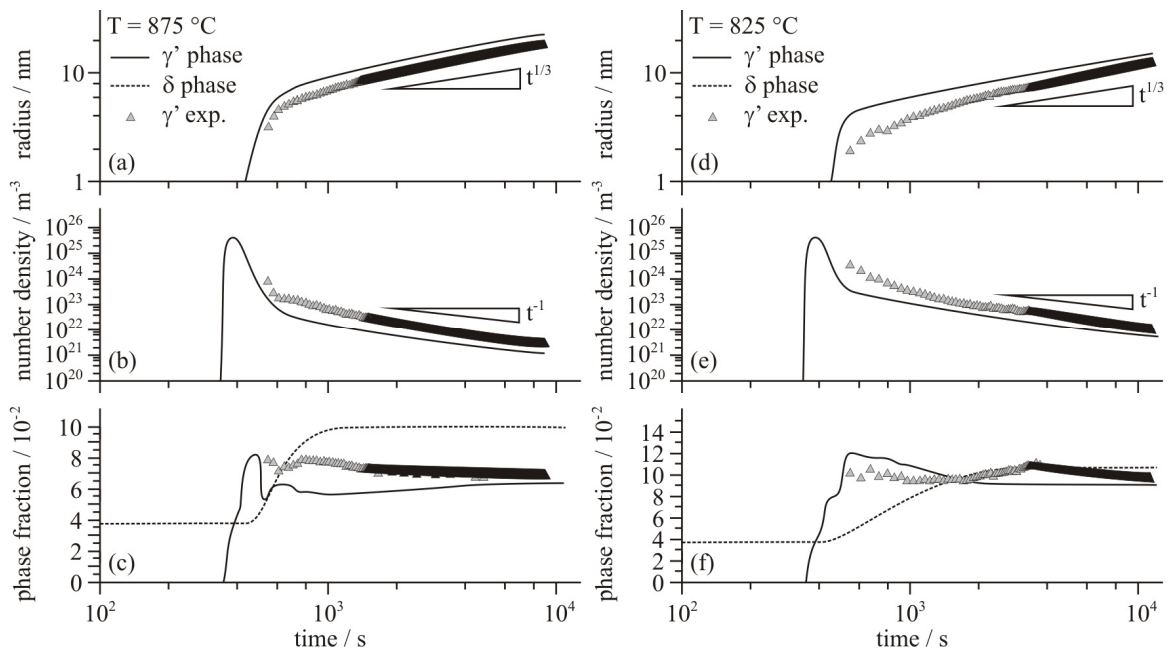


Figure 4: Radius, number density and volume fraction of γ' precipitates versus time and comparison with experimental results [24] at temperatures of 825 °C and 875 °C.

However, using the thermodynamic database [10], the simulation of the solution heat treatment according to ref. [24] predicts residual δ phase precipitates in the initial stages of isothermal annealing, see the phase fraction curves of δ phase precipitates in Figure 4(c,f). Thus, no calculated information can be provided regarding the precipitate parameters mean radii and number density, since these parameters are not defined in the initial stage of the calculation due to the incomplete dissolution of the particles after solution treatment of the as received material.

The radius of the γ' precipitates increases with aging time and the growth rate is proportional to $t^{1/3}$ in the late stages (Figure 4(a,d)). The number density of the γ' precipitates leaps to values of about 10^{26} m^{-3} , followed by a continuous decrease with a proportionality to t^{-1} in the late stages of precipitation (Figure 4(b,e)). The volume fraction of the precipitates (Figure 4(c,f)) increases simultaneously with the number density followed by a partial redissolution, supporting growth of the thermodynamically more stable δ phase, similar to the observations depicted in Figure 3(f). The kinetics of the γ' precipitates indicates classical Ostwald ripening, which is described in detail in reference [24]. Additional calculations of the precipitation kinetics of γ' in ATI Allvac@718PlusTM at annealing temperatures of 850 °C and 900 °C can be found in ref. [25].

Both, Figure 3 as well as Figure 4 indicate, that, below the supersolvus temperature of γ' , the precipitation kinetics of δ is influenced by the precipitation of γ' and vice versa. The simultaneous precipitation of both phases leads to a competition of Nb and Al with respect to the δ and γ' formation. It should be emphasized that a certain amount of Nb is not unusual in γ' precipitates, which is reported in refs. [26,27], where the chemical composition of γ' in alloy 718 is investigated theoretically with thermodynamic calculations and experimentally by atom probe investigations.

Depending on temperature and time, Al and Nb atoms redistribute to achieve optimum thermodynamic conditions. This is clearly demonstrated in Figure 5, where the phase fractions of the δ and γ' phases (a) and the mole atoms of Al and Nb in these phases (b) are plotted versus time for an annealing temperature of 850 °C, according to the calculation shown in Figure 3(f) [23].

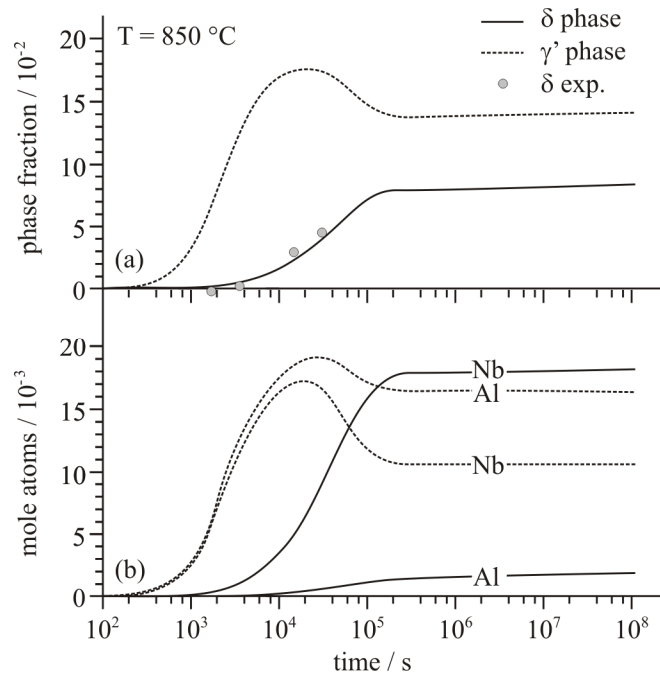


Figure 5: Calculated phase fractions of the γ' and δ phases (a) as well as the mole atoms of Al and Nb in these phases (b) versus time at a temperature of 850 °C [23].

After rapid precipitation, partial redissolution of γ' is observed, supporting the growth of the δ phase. Therefore, Nb and Al atoms, previously bonded in γ' , are redistributed by diffusional transport, which leads to an increase of the δ phase. At higher aging temperatures above the γ' precipitation, no competitive diffusion process occurs, resulting in faster precipitation of the δ phase, which has been verified experimentally, see Figure 3.

Finally, Figure 6 shows the calculated time-temperature-precipitation (TTP) diagram for both, the δ and γ' phases in ATI Allvac® 718Plus™ [23]. The solid lines mark phase fractions of 2 and 5 vol. % of δ phase, the dashed lines represent 2 vol.% of γ' phase. The calculated results for the δ phase are compared to experimental data (2 vol.% and 5 vol.%). The nose temperature for δ phase precipitation is observed at 950 °C, the calculated nose temperature for γ' precipitates is 730 °C. The rapid precipitation of γ' , faster than the precipitation of δ , leads to a delay in the precipitation kinetics of δ and a discontinuity in the C-curves of the time-temperature-precipitation diagram.

To verify the calculated TTP diagram at lower temperatures, additional experimental investigations are suggested for the future. The numerical calculations at temperatures above 850 °C show excellent agreement with the experimental investigations.

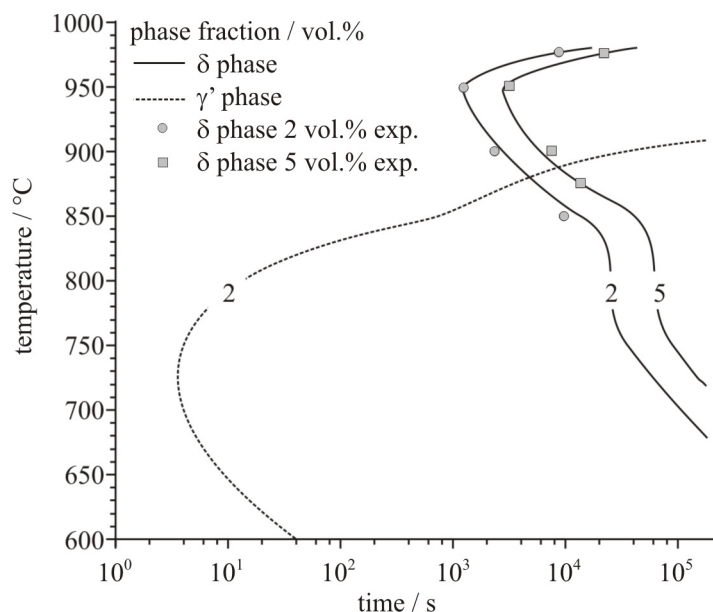


Figure 6: Calculated time-temperature-precipitation plot of δ and γ' phases and comparison with experimental results for the δ phase [23].

Summary

The present work deals with the numerical analysis of the precipitation kinetics of δ and γ' phases in the nickel-base superalloy ATI Allvac® 718Plus™. Precipitation kinetics simulations at different temperatures are performed with the thermo-kinetic software MatCalc. The theoretical investigations are compared with experiments. To match the observed kinetics, the predicted interfacial energy of precipitates of planar, sharp interfaces is adjusted to smaller values at temperatures close to the solubility temperature. Using these modified interfacial energies, the calculated results show excellent agreement with the experimental measurements. Finally, a complete time-temperature-precipitation (TTP) diagram is calculated. The TTP plot shows C-shaped curves with characteristic discontinuities in the temperature range, where both

phases precipitate simultaneously. The discontinuity is attributed to the competition in diffusional transport of Nb and Al to the γ' and δ precipitates. Thus, the present work gives important information for controlling the heat treatment parameters temperature and time during processing, in order to achieve the desired material properties.

References

1. C.T. Sims, N.S. Stoloff, and W.C. Hagel, *Superalloys II*, (New York, NY, USA: John Wiley & Sons, 1987).
2. W.D. Cao, and R. Kennedy, "Role of Chemistry in 718-Type Alloys - Allvac®718plus™ Alloy Development," *Proceedings of the International Symposium on Superalloys 2004*, eds. K.A. Green, T.M. Pollock, H. Harada, T.E. Howson, R.C. Reed, J.J. Schirra, and S. Walston (Warrendale, PA, USA: The Minerals, Metals and Materials Society, 2004), 91-99.
3. C. Stotter, C. Sommitsch, J. Wagner, H. Leitner, I. Letofsky-Papst, G.A. Zickler, W. Prantl, and M. Stockinger, "Characterization of δ -Phase in Superalloy Allvac 718Plus™," *International Journal of Materials Research*, 99(4) (2008), 376-380.
4. V. Beaubois, J. Huez, S. Coste, O. Brucelle, and J. Lacaze, "Short Term Precipitation Kinetics of Delta Phase in Strain Free Inconel® 718 Alloy," *Materials Science and Technology*, 20(8) (2004), 1019-1026.
5. E. Nembach, and G. Neite, "Precipitation Hardening of Superalloys by Ordered γ' -Particles," *Progress in Materials Science*, 29(3) (1985), 177-319.
6. A.J. Ardell, "Precipitation Hardening," *Metallurgical Transactions A*, 16(12) (1985), 2131-2165.
7. J. Svoboda, F.D. Fischer, P. Fratzl, and E. Kozeschnik, "Modelling of Kinetics in Multi-Component Multi-Phase Systems with Spherical Precipitates I: Theory," *Materials Science and Engineering A*, 385(1-2) (2004), 166-174.
8. E. Kozeschnik, J. Svoboda, P. Fratzl, and F.D. Fischer, "Modelling of Kinetics in Multi-Component Multi-Phase Systems with Spherical Precipitates II: Numerical Solution and Application," *Science and Engineering A*, 385(1-2) (2004), 157-165.
9. E. Kozeschnik, J. Svoboda, and F.D. Fischer, "Modified Evolution Equations for the Precipitation Kinetics of Complex Phases in Multi-Component Systems," *CALPHAD-Computer Coupling of Phase Diagrams and Thermochemistry*, 28(4) (2005), 379-382.
10. ThermoTech, Ni-Database Version 5.0, <http://www.thermotech.co.uk/databases.html> (19.01.2009).
11. C.E. Campbell, W.J. Boettinger, and U.R. Kattner, "Development of a Diffusion Mobility Database for Ni-Base Superalloys," *Acta Materialia*, 50(4) (2002), 775-792.
12. K. Russell, "Nucleation in Solids - The Induction and Steady-State Effects," *Advances in Colloid and Interface Science*, 13(3-4) (1980), 205-318.

13. K.G.F. Janssens, D. Raabe, E. Kozeschnik, M.A. Miodownik, and B. Nestler, *Computational Materials Engineering – An Introduction to Microstructure Evolution* (Oxford, UK: Elsevier Academic Press, 2007).
14. E. Kozeschnik, J. Svoboda, and F.D. Fischer, “On the Role of Chemical Composition in Multi-Component Solid-State Nucleation,” *Proceedings of an International Conference on Solid-Solid Phase Transformations in Inorganic Materials*, eds. J.M. Howe, D.E. Laughlin, J.K. Lee, U. Dahmen, and W.A. Soffa, (Phoenix, AZ, USA: The Minerals, Metals and Materials Society, 2005), 301-310.
15. R. Radis, M. Schaffer, M. Albu, G. Kothleitner, P. Pölt and E. Kozeschnik, “Multimodal Size Distributions of γ' Precipitates During Continuous Cooling of UDIMET 720 Li,” *Acta Materialia* 57(19) (2009), 5739–5747.
16. R. Kampmann, and R. Wagner, “Kinetics of Precipitation in Metastable Binary Alloys - Theory and Applications to Cu-1.9 at% Ti and Ni-14 at% Al.,” *Decomposition of Alloys: The Early Stages, Proceedings of the 2nd Acta-Scripta Metallurgica Conference*, eds. P. Haasen, V. Gerold, R. Wagner, M.F. Ashby, (Oxford, UK: Pergamon Press, 1983), 91-103.
17. B. Sonderegger, and E. Kozeschnik, “Generalized Nearest-Neighbor Broken-Bond Analysis of Randomly Oriented Coherent Interfaces in Multicomponent Fcc and Bcc Structures,” *Metallurgical and Materials Transactions A*, 40(3) (2009), 499-510.
18. M. Pudar, E. Kozeschnik, A. Sormann, and E. Parteder, “Numerical Analysis of the Nb(CN) Precipitation Kinetics in Microalloyed Steels,” *Steel Research International*, 79(8) (2008), 660-664.
19. R. Radis, and E. Kozeschnik, “Concurrent Precipitation of AlN and VN in Microalloyed Steel,” *Steel Research International*, (2010), accepted.
20. Y.W. Lee, and H.I. Aaronson, “Anisotropy of Coherent Interphase Boundary Energy,” *Acta Metallurgica*, 28(4) (1980), 539-48.
21. B. Sonderegger, and E. Kozeschnik, “Size Dependence of the Interfacial Energy in the Generalized Nearest-Neighbor Broken-Bond Approach,” *Scripta Materialia*, 60(8) (2009), 635-638.
22. D. Hull, and D.J. Bacon, *Introduction to Dislocations* (Oxford, UK: Pergamon Press Ltd., 1984).
23. R. Radis, G.A. Zickler, M. Stockinger, C. Sommitsch, E. Kozeschnik, “Interaction of the Precipitation Kinetics of δ and γ' Phases in Nickel-Base Superalloy ATI Allvac®718Plus™,” *Materials Science Forum* 638-642 (2010), 2712-2717.
24. G.A. Zickler, R. Schnitzer, R. Radis, R. Hochfellner, R. Schweins, M. Stockinger, and H. Leitner, “Microstructure and Mechanical Properties of the Superalloy ATI Allvac®718Plus™,” *Materials Science and Engineering A* 523(1-2) (2009), 295-303.

25. G.A. Zickler, R. Radis, R. Schnitzer, E. Kozeschnik, M. Stockinger, and H. Leitner, "The Precipitation Behavior of Superalloy ATI Allvac 718Plus," *Advanced Engineering Materials*, 12 (2010), 176-183.
26. K. Wu, F. Zhang, S. Chen, W. Cao, and Y.A. Chang, "A Modeling Tool for the Precipitation Simulations of Superalloys During Heat Treatments," *Proceedings of the International Symposium on Superalloys 2008*, eds. R.C. Reed, K.A. Green, P. Caron, T.P. Gabb, and M.G. Fahrman, (Warrendale, PA, USA: The Minerals, Metals and Materials Society, 2008), 933-939.
27. M.K. Miller, and S.S. Babu, "Atomic Level Characterization of Precipitation in Alloy 718," *Proceedings of the International Symposium on Superalloys and Various Derivatives*, ed. E.A. Loria, (Warrendale, PA, USA: The Minerals, Metals and Materials Society, 2001), 357-365.